Korean Journal of Chemical Engineering
https://doi.org/10.1007/s11814-026-00648-9

ORIGINAL ARTICLE

Dissolution Behavior and Kinetics of Insulating Glass Wool Under Highly Alkaline Conditions

Kiwon Kang[1] · Changhyun Shim[1] · Yulim Lee[1] · Hyeongjin Byeon[2] · Jaeyeong Park[1]

Received: 10 November 2025 / Revised: 1 January 2026 / Accepted: 7 January 2026

Abstract

This study aimed to evaluate the long-term stability of glass wool used as insulation material in domestic nuclear power plants and to quantify its degradation mechanisms and dissolution kinetics under highly alkaline conditions (pH≥12) expected in cementitious environments associated with vault-type disposal systems for low-level radioactive waste. Experiments were conducted at 20 °C and 80 °C using cement-saturated groundwater (CGW) as the primary solution, while comparative tests were performed in NaOH and $Ca(OH)_2$ solutions at equivalent pH levels. ICP-OES, SEM-EDS, and XRD analyses revealed that dissolved Ca^{2+} significantly suppressed glass dissolution. The presence of abundant Ca^{2+} ions promoted densification of the surface alteration layer, retarding degradation, whereas depletion of Ca^{2+} resulted in a rapid increase in the dissolution rate. Although calcium silicate hydrate (CSH) precipitates are generally known to inhibit glass corrosion, the CSH phases formed in this study exhibited limited protective capability due to their low Ca/Si ratios and high porosity. Based on the dissolution rate constant at 20 °C, the complete dissolution of glass wool was estimated to require approximately 213 years; however, under conditions of limited Ca^{2+} availability, the dissolution rate could increase by up to 70-fold, approaching that observed in NaOH solution.

Keywords Glass wool · Glass degradation · Dissolution kinetics · Waste disposal · Cement-saturated groundwater

Introduction

Glass wool is lightweight, non-combustible, and exhibits excellent thermal insulation performance, making it one of the most widely used insulating and heat-preserving materials in construction and industrial facilities [1, 2]. In domestic nuclear power plants (NPP), glass wool has long been used to insulate pipes and equipment. As domestic nuclear facilities move toward decommissioning, the need for the disposal and long-term stability assessment of these insulation materials is increasing. Because of its relatively low levels of radioactivity, glass wool used as insulation in NPPs is expected to be disposed of in near-surface facilities for low-level radioactive waste, such as vault-type repositories. These disposal systems commonly consist of concrete-based engineered barriers and closures that are likely to generate highly alkaline pore water (pH > 12) over extended timescales following closure. Numerous studies have documented that under such high-pH conditions, the silicate glass network constituting glass wool undergoes more rapid and sustained dissolution than in typical groundwater environments [3–6]. Therefore, it is essential to evaluate the long-term stability of glass wool insulation under disposal conditions and to characterize its degradation mechanisms and long-term dissolution rates. In domestic vault-type radioactive waste repositories, the presence of concrete-based engineered barriers results in highly alkaline groundwater chemistry [7]. Consequently, infiltrating groundwater in contact with the glass wool is expected to become strongly alkaline (pH ≈ 12–13) with elevated ionic strength, owing to the leaching of alkali (e.g., Na^+, K^+) and alkaline earth (Ca^{2+}) metal ions from the concrete, accompanied by high OH^- activity.

Kiwon Kang and Changhyun Shim contributed equally to this work.

✉ Jaeyeong Park
jypark@unist.ac.kr

[1] Department of Nuclear Engineering, Ulsan National Institute of Science and Technology, 50 UNIST-gil, Ulsan 44919, Republic of Korea

[2] Korea Atomic Energy Research Instituite, 111 Daedeok-daero 989 beon-gil, Yuseong-gu, Daejeon 34057, Republic of Korea

Published online: 03 February 2026

The glass network generally consists of a network former (e.g., SiO_2, B_2O_3, and, in some cases, Al_2O_3), together with weakly bonded network modifiers (e.g., Na_2O, K_2O, CaO, or MgO). Under such highly alkaline conditions, the dissolution and degradation behaviors of glass wool can be described by two principal mechanisms. The first is interdiffusion, an incongruent dissolution process in which modifier species in the glass network (e.g., Na^+, K^+, and Ca^{2+}) are exchanged with cations in solution and released without directly breaking the silica framework. Although interdiffusion does not directly attack the silica network, compositional depletion and subsequent interactions with the solution can contribute to mass loss. The second mechanism is network hydrolysis, in which hydroxide ions attack siloxane ($\equiv Si - O - Si \equiv$) bonds, leading to depolymerization of the silicate framework and resulting in congruent dissolution behavior. When interdiffusion prevails, the dissolution rate is limited by mass transport, whereas when hydrolysis prevails, it is limited by surface reactions, with both mechanisms potentially acting in parallel. As glass alteration proceeds, systems commonly transition from a maximum forward-rate (initial-rate) regime, in which interdiffusion and network hydrolysis operate in parallel, to a residual-rate regime controlled by transport, as a result of the formation of an altered layer and the affinity effect. However, under strongly alkaline conditions, the rate remains elevated even in the residual stage, as network hydrolysis continues to be the rate-determining step [6]. Therefore, under conditions that minimize the affinity effect associated with silica saturation, elevated temperature, and high liquid-to-solid ratio, the glass network typically dissolves at an approximately constant rate. This dissolution rate can then be determined using several approaches, including (i) gravimetric mass loss [8], (ii) solution-based normalized mass loss (NL) for a relatively conservative network-forming element (e.g., Si or B) [9–11], and (iii) diameter-reduction kinetics, especially for glass fibers [6, 12]. Under disposal conditions, advective groundwater flow renews the solution and limits silica accumulation, making the chemistry comparable to that of the L/S test that minimizes the affinity effect. As a conservative assumption, a constant rate was used as an upper-bound reference for the repository-relevant kinetics.

Glass network dissolution reflects a combined dependence on pH and the compositions of both the glass and the solution; thus, dissolution rates may diverge even at identical pH values under otherwise comparable test conditions. Under the same pH conditions, Bashir et al. [6] measured the dissolution rate of E-glass in NaOH and KOH and found that it was approximately twice as high in NaOH. This phenomenon indicates that hydroxide activity in solution depends on the cations present. In addition, at the same pH in an NaOH solution matrix, La Plante et al. [11] showed that the dissolution rate was highly sensitive to the added electrolyte, varying more than fivefold across electrolyte type and concentration. Notably, the addition of electrolytes bearing divalent cations (Ca^{2+} and Mg^{2+}) led to a pronounced suppression of the dissolution rate. The addition of divalent cations, such as Ca^{2+} and Mg^{2+}, significantly decreases the dissolution rate, implying that these cations increase the activation barrier for Si–O bond rupture and reduce surface reactivity through Ca–Si interactions. The influence of dissolved Ca ions on glass network dissolution mechanisms has been investigated in several studies [3, 10, 13]. Mercado-Depierre et al. measured the initial dissolution rates of borosilicate glass across varying pH values with and without Ca ions. At pH < 10.5, adding Ca increased the rate relative to the Ca-free solution (about 4.4 × at pH 7 and 1.8 × at pH 10), whereas at pH ≥ 11 the rate decreased below the Ca-free baseline (about 6.5 × lower at pH 11.7). These trends indicate pH-dependent Ca–Si interactions at the interface and within the altered layer: at lower pH, complexation by Ca can enhance dissolution, while at higher pH, Ca–Si interactions promote the formation of a passivating layer that suppresses further dissolution.

For similar reasons, interfacial secondary precipitates and altered-layer passivation are strongly dependent on the glass composition. The species released from the glass network (primarily Si, Al, Na, Ca, and Mg) reprecipitate as secondary phases. In strongly alkaline environments, the representative products include amorphous silica, calcium silicate hydrate (CSH) [14, 15], zeolites [16], brucite [9], and portlandite ($Ca(OH)_2$) [17]. The influence of these precipitates on dissolution rates is complex and system dependent. In closed systems, the formation of secondary precipitates can consume dissolved silica, thereby mitigating the affinity effect and promoting additional dissolution of the glass network. This phenomenon is commonly referred to as alteration resumption. Interfacial CSH on glass exhibits compositions ranging from amorphous to Ca-rich (higher Ca/Si) and Si-rich (lower Ca/Si), which differentially affect glass–solution interactions. Amorphous or Si-rich CSH has been reported to have little to no effect on the dissolution rate [9, 17, 18], whereas Ca-rich CSH forms a passivating interphase that substantially reduces dissolution [19, 20]. In addition, the secondary CSH phase is susceptible to carbonation in the presence of carbonate ions (or dissolved carbon dioxide). Carbonation alters the mineralogical structure and continuity of the CSH interphase, thereby modifying

its protective capacity against further glass dissolution. The resistance of CSH to carbonation increases with higher Ca/Si ratio, indicating that both Ca availability and carbonate concentration jointly control the stability and effectiveness of the passivating layer [21–24]. In vault-type repository environments, carbonate species (e.g., HCO^{3-}/CO_3^{2-}) are expected to be present in groundwater and the groundwater is anticipated to interact with cement-based engineered barriers, leading to the formation of cement-saturated groundwater (CGW) enriched in Ca and carbonate species. These conditions can further influence interfacial reactions at the glass surface. Consequently, variations in the glass and solution compositions, particularly with respect to dissolved Ca and Carbonate concentrations, can lead to differences in dissolution behavior and rates. Therefore, accurate assessment of silicate glass degradation requires experimental evaluation using solution chemistries that realistically represent the intended disposal environment.

This study investigated the degradation mechanisms of insulation-grade glass wool previously used in NPPs under strongly alkaline conditions and quantified its dissolution rates under simulated vault-type repository-relevant solution chemistries. The glass wool used in domestic NPPs was tested. To simulate repository-proximal conditions, groundwater collected near the disposal site was saturated with cement (cement-saturated groundwater) and used as the primary solution. Unlike deep geological repositories or silo-type systems, vault-type near-surface repositories are expected to maintain partial interaction with the atmosphere and infiltrating groundwater over long timescales, resulting in non-negligible dissolved CO_2 and carbonate concentrations in groundwater. Accordingly, carbonate-bearing conditions were intentionally preserved rather than excluded, in order to capture the potential influence of carbonation on secondary phase formation, passivation behavior, and long-term dissolution kinetics. For comparison across alkaline solutions, NaOH and $Ca(OH)_2$ solutions were prepared at the same pH and subjected to identical tests. To assess long-term behavior within practical timescales, accelerated degradation experiments were conducted at elevated temperature (80 °C), and separate measurements were performed to determine dissolution rates under repository-representative conditions (20 °C). Time-resolved characterization of the surface morphology, secondary precipitates, and solution chemistry was performed using standard analytical techniques.

Experimental Procedures

Materials

Characterization of Glass Wool

The glass wool (labeled as GW) used in this study has been utilized as an insulation material in domestic nuclear power plants. The composition of the glass wool was analyzed using X-ray Fluorescence (XRF; S8 Tiger, Bruker), and the results are shown in Table 1. Based on its oxide composition, the glass wool used in this study was classified as soda-lime silicate glass.

To examine the presence of additional crystalline materials within the fibers, high-resolution powder X-ray diffraction (HRPXRD; SmartLab, Rigaku) was performed on finely ground fiberglass. The analysis results indicated that the insulating glass wool is completely amorphous, with no detectable crystalline phases (Fig. 1). The specific surface area (SSA) of the glass wool was determined by nitrogen adsorption using the Brunauer–Emmett–Teller (BET) method (BELSORP-MAX, MicrotracBEL), yielding a value of 0.63267 m²/g. Scanning electron microscopy (SEM) was performed at several positions on the glass wool, from which more than 100 fiber diameters were measured to compute the mean. The average initial diameter of the glass wool before the experiment was 7.66 ± 0.59 μm.

Glass Wool Dissolution Tests

Solution Preparation

To compare the dissolution behavior of glass wool under various alkaline conditions, three solutions at pH 12.5—NaOH, $Ca(OH)_2$, and cement-saturated groundwater (hereafter CGW)—were prepared and used in the experiments. NaOH and $Ca(OH)_2$ solutions were prepared by dissolving analytical-grade NaOH and $Ca(OH)_2$ pellets in deionized water. The CGW was produced using groundwater collected from the Gyeongju area, where the national disposal facility is located. The groundwater was brought into contact with ordinary Portland cement (OPC, Type I) powder while minimizing exposure to ambient air. To preserve the composition of the groundwater sampled under reducing conditions, CO_2 ingress was minimized throughout the preparation process by sealing the containers and purging them with N_2.

Table 1 Elemental composition and physical properties of glass wool used in this study

Sample	Oxide composition							Density (g/cm^3)	SSA (m^2/g)	Diameter (μm)
	SiO_2	Na_2O	CaO	MgO	Fe_2O_3	Al_2O_3	Others			
Glass wool	64.4	17.2	9.9	2.2	2.15	3.22	0.93	2.38	0.63267	7.66 ± 0.59

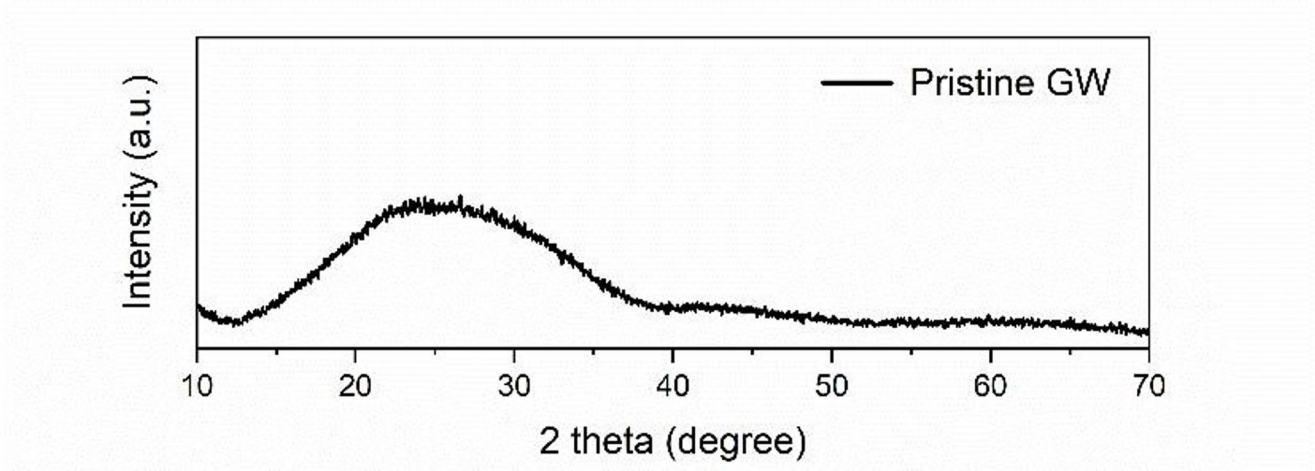

Fig. 1 X-ray diffraction (XRD) pattern of the as-received glass wool prior to dissolution experiments

Table 2 Chemical composition and pH of groundwater collected under reducing conditions in the Gyeongju area

Solution	pH	Cation concentration (mg/L)				Anion concentration (mg/L)		
		Na	Ca	Mg	K	Cl	SO_4	F
Groundwater	7.12	30.50	47.28	8.64	2.93	24.67	94.11	-
CGW	12.5	63.83	348.03	0.25	376.77	52.21	443.41	0.62

After reaching the target pH, the supernatant was filtered through a 0.45 µm PTFE membrane and used for testing. The major ionic constituents of the solution (Na, K, Ca, Mg, Cl, and SO_4^{2-}) were quantified using inductively coupled plasma-optical emission spectrometry (ICP-OES) and ion chromatography (IC). The chemical composition and pH of the groundwater before and after cement saturation are summarized in Table 2.

Dissolution Experiments

Dissolution experiments were conducted based on the Product Consistency Test (PCT, ASTM C1285-21) framework [25], which is used to assess the durability of ceramic materials. Among PCT-A and PCT-B, the present study employed PCT-B, which allows flexible adjustment of experimental conditions such as temperature and duration. The experimental vessels were made of perfluoroalkoxy (PFA) Teflon, which maintains integrity under highly alkaline and high-temperature conditions. To simulate carbonate-bearing conditions, a closed system was configured with a headspace-to-solution volume ratio of 1:1. This setup prevented external CO_2 ingress while allowing initial equilibrium dissolution of CO_2 into the solution. All experiments were conducted in static batch mode at a liquid-to-solid (L/S) mass ratio of 100. Three alkaline solutions adjusted to pH 12.5 were used. Two temperature sets were employed: 80 °C to examine accelerated degradation and persistence of dissolution, and 20 °C to establish baseline dissolution rates representative of domestic repository conditions. For the high-temperature accelerated tests, vessels containing only solution were preheated at the target temperature for 24 h in a temperature-controlled chamber before the addition of glass wool, given the low thermal conductivity of PFA. The experimental conditions are listed in Table 3.

Table 3 Experimental parameters for the dissolution of glass wool in alkaline solutions

Experiment objective	Solution (pH)	Temperature (°C)	Dissolution time
Accelerated dissolution experiment	NaOH (12.5) $Ca(OH)_2$ (12.5) CGW (12.5)	80	1, 3, 6, 12, 24, 72 h 7, 14, 20, 30 days
Dissolution kinetics under repository-simulated conditions	CGW (12.5) NaOH (12.5)	20	3, 5, 7, 15, 20, 30 days

Samples were labeled according to the format ${}^{temperature}_{exposure\ time}GW_{solution}$. Here, GW denotes the glass wool; Na = NaOH, Ca = $Ca(OH)_2$, and CGW = cement-saturated groundwater. For example, ${}^{80}_{7d}GW_{Na}$ refers to a glass wool sample exposed to NaOH at 80 °C for 7 days.

Analytical Methods

SEM–EDS Analysis

After the dissolution experiments, the specimens were immediately immersed in deionized (DI) water and gently cleaned to prevent further dissolution by residual solution. The samples were then rapidly dried in a vacuum chamber prior to analysis. The washed specimens were examined using a scanning electron microscope (SEM; SU-8220, Hitachi) to observe surface morphology. Considering the working distance (WD), wool pieces were arranged to avoid overlap within the field of view and to place as many fibers as possible on the focal plane. To mitigate surface charging, the specimens were sputter-coated with Pt. Imaging and energy-dispersive X-ray spectroscopy (EDS; E-1045, Hitachi) were performed at 5 and 15 kV, respectively. Given the topography and coating-induced X-ray absorption on rough wool surfaces, the EDS data were interpreted semi-quantitatively. Analyses were performed at five or more locations within regions exhibiting similar features (precipitate layer and spheroidal precipitates), and the average value was used.

ICP–OES Analysis

Post-experiment solution chemistry was analyzed using inductively coupled plasma-optical emission spectrometry (ICP–OES; iCAP Pro, Thermo Fisher). Silicon (to estimate dissolution rate), calcium, and sodium (to track solution composition changes) were quantified. Prior to analysis, solutions were filtered through 0.45 μm PTFE membranes and acidified with nitric acid (HNO_3).

XRD Analysis

Phase identification of corrosion products was conducted using powder X-ray diffraction (SmartLab; Rigaku) at 40 kV and 200 mA. Patterns were collected over 10–70° with a step size of 0.02°. Phases were identified using PDXL2 software with the ICDD database (PDF-2, 2021).

Calculation of Normalized Mass Loss and Dissolution Rate

From the measured solution concentrations and specific surface area of the GW, the amount of element i released by dissolution (e.g., Si, Ca, Na) was converted to the normalized mass loss, NL_i ($\mu g/cm^2$), using Eq. 1:

$$NL_i = \frac{C_i * V * 1000}{SSA * m * X_i} \tag{1}$$

where C_i is the concentration (mg/L) of element i in solution, V is the solution volume (L), SSA is the initial specific surface area of the glass wool (cm^2/g), m is the glass wool mass (g) immersed in the solution, and X_i is the mass fraction of element i in the GW. By multiplying Eq. (1) by the specific surface area, the mass-normalized specific release of element i, SR_i, is obtained (Eq. 2):

$$SR_i = \frac{C_i * V}{m * X_i} \tag{2}$$

As Si (or SiO_2) is the principal network former in silicate glass, the Si release rate is widely used as an indicator of overall glass network dissolution [26]. Following Thelohan and de Meringo [27], the dissolution rate of the silica network, ν (nm/day), is given by:

$$\nu = \frac{d}{2t\left(1 - \sqrt{1 - SR_{Si}}\right)} \tag{3}$$

where d is the glass fiber diameter (nm), and t is the total dissolution time (days).

If the solution analysis indicates congruent dissolution of the silicate network, ν can be taken as the global dissolution rate. Under this assumption, the dissolution rate constant $k_{dissolution}$ (typically reported in $ng/cm^2 \cdot h$) and time to complete dissolution $t_{dissolution}$ (days) are given by:

$$k_{dissolution} = \left(\frac{\rho}{0.24}\right)\nu \tag{4}$$

$$t_{dissolution} = \frac{2083.3 \times \rho}{k_{dissolution}} \times d \tag{5}$$

where ρ is the glass fiber density (g/cm^3), 0.24 is total conversion factor (days → hours and geometric unit conversions).

As noted in prior studies, early-time transient arising from non-congruent release and/or secondary precipitation causes substantial variability in ν, which diminishes as the system approaches a quasi-steady state [26]. Accordingly, $k_{dissolution}$ was evaluated from ν at 14, 20, and 30 days, and the mean of these three values was used to estimate $t_{dissolution}$, following established methodologies.

Results and Discussion

Surface Morphology Analysis (SEM-EDS, XRD)

The microstructures of the glass wool were examined using SEM. Prior to the degradation tests, the glass wool surfaces were smooth, with no visible cracks or pores (Fig. 2). To examine surface alteration over time, specimens were retrieved at the dissolution intervals listed in Table 3 under accelerated degradation conditions. The surface morphology was characterized by SEM and EDS, and the precipitated phases were identified using X-ray diffraction (XRD).

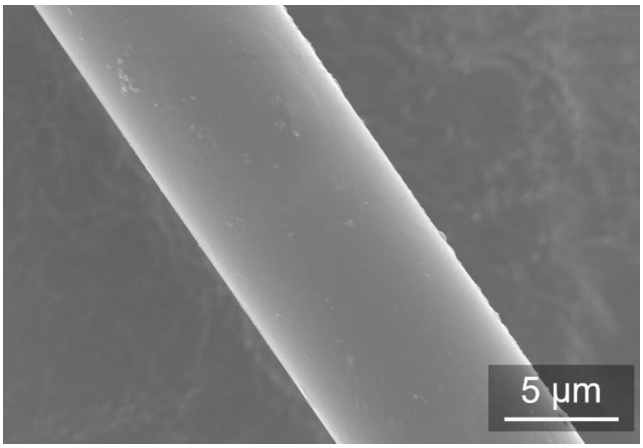

Fig. 2 SEM image of the as-received glass wool before dissolution experiments

Surface Alterations in $Ca(OH)_2$ Solution

Microstructural observations and XRD analysis revealed no surface alterations or precipitate formation on the ${}^{80}_{30d}GW_{Ca}$ sample. This finding is consistent with the solution analysis results, indicating negligible surface change in $Ca(OH)_2$ solution under accelerated degradation conditions (80 °C) (Fig. 3).

Similar observations have been reported in previous studies: when the concentration of dissolved Ca^{2+} in the solution was sufficiently high, silicate glass degradation proceeds very slowly. Ca^{2+} can penetrate the amorphous hydrated surface layer, leading to calcium condensation within the layer [28, 29]. XPS analyses confirm the formation of a Ca-enriched layer a few nanometers thick, which limits ion transport and inhibits further glass degradation. Molecular-level simulations by Liu et al. demonstrated that divalent cations promote Si–O–M^{2+} bond formation, increasing the hydrolysis energy barrier and slowing dissolution reaction [30]. This results in a passivating reactive interphase (PRI) that suppresses diffusion and surface reactions [17]. Although localized pitting has been reported in previous studies, no such behavior was observed here after 30 days at 80 °C [31] (Fig. 4).

Surface Alterations in NaOH Solution

SEM analyses of specimens collected at the intervals listed in Table 3 revealed pronounced surface alterations in NaOH solution, unlike in $Ca(OH)_2$ at the same pH, where such changes were negligible. The initial morphology of GW is shown in Fig. 5, and alterations up to 30 days are presented in Fig. 6.

After 6 h of exposure, ${}^{80}_{6h}GW_{Na}$ exhibited nanoporous surfaces with small pits, likely due to preferential dissolution of network-modifying elements (Na, Ca, Al, Mg, K) from the glass network [32]. The dissolution process is driven by reactions between OH^- ion and network-modifiers that are relatively weakly bonded within the glass structure. As dissolution proceeds, the formation of pits results in an increase in surface porosity. Because the porous layer was

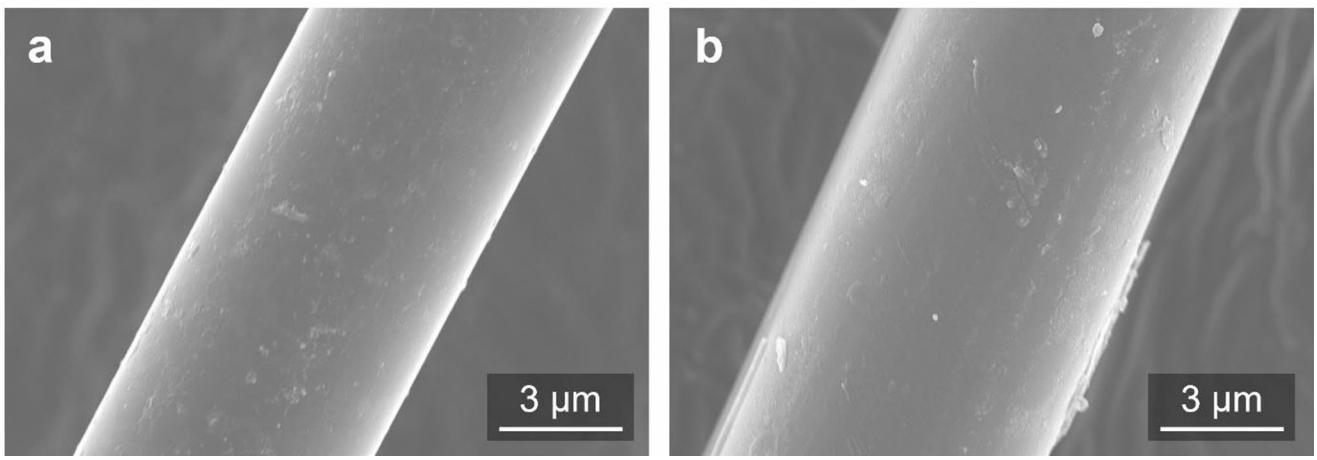

Fig. 3 SEM micrographs of glass wool fiber surfaces after accelerated degradation in $Ca(OH)_2$ solution: (**a**) 7 days and (**b**) 30 days

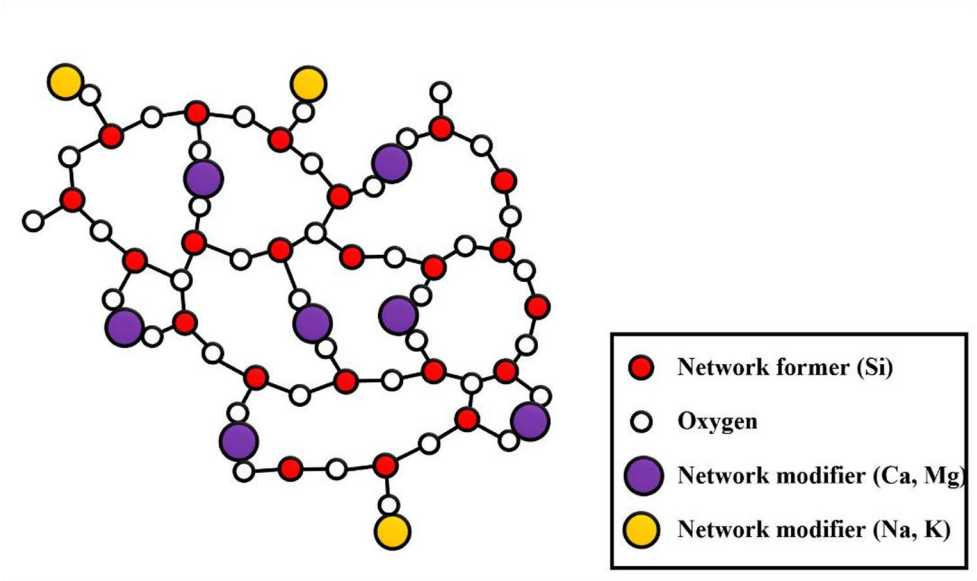

Fig. 4 Schematic representation of the atomic structure of a typical glass

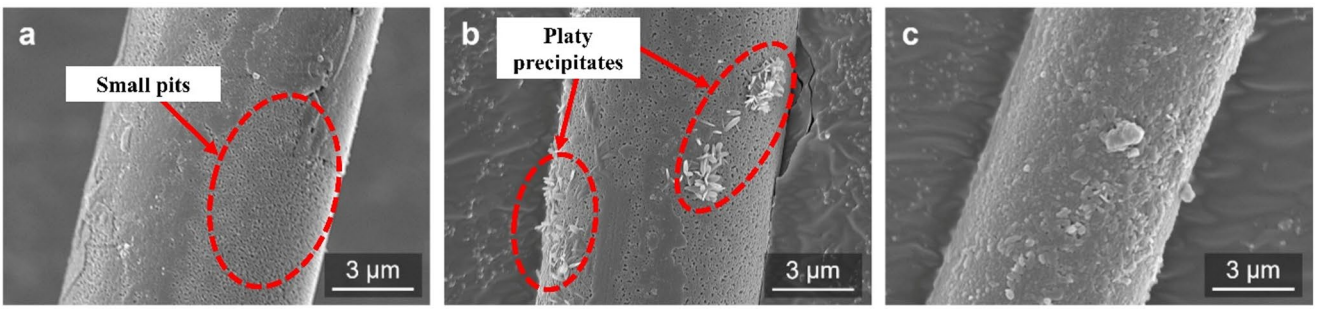

Fig. 5 SEM micrographs of glass wool fiber surfaces after accelerated degradation in NaOH solution: (**a**) 6 h, (**b**) 12 h, and (**c**) 24 h

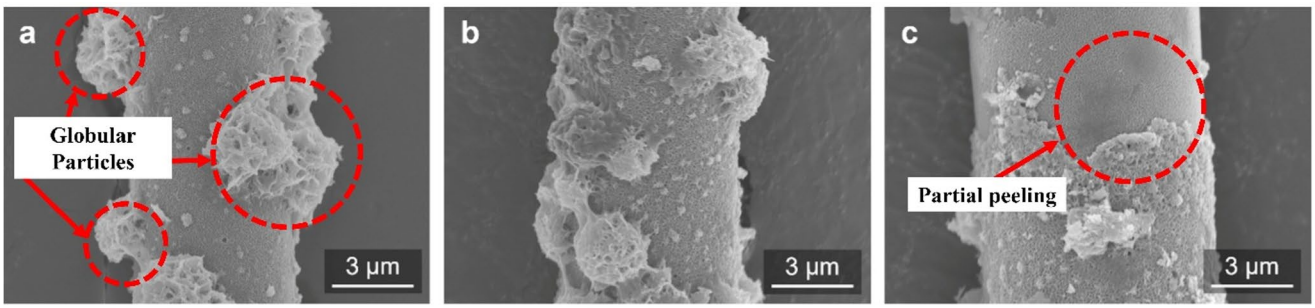

Fig. 6 SEM micrographs of glass wool fiber surfaces after accelerated degradation in NaOH solution: (**a**) 7 days, (**b**) 14 days, and (**c**) 30 days

located at the same interface as the original GW core surface, this suggests that surface modification occurred within the original layer rather than through the formation of a new precipitated layer.

By 12 h, most surfaces were porous, with localized precipitates (Fig. 5b). These precipitates exhibited thin platy morphologies (~1–2 µm), consistent with crystalline CSH (tobermorite). In some ${}^{80}_{24h}GW_{Na}$ specimens, the amorphous nanoparticles precipitated and aggregated over the preexisting porous alteration layer, forming an interconnected percolating network.

In the ${}^{80}_{7d}GW_{Na}$, most of the GW surfaces were covered by a platelet-structured layer, and additional microscale globular- or dome-shaped amorphous particles were formed (Fig. 6a). These particles exhibited a highly porous, open-framework surface and irregular spherical morphology composed of platy or foil-like units stacked in a disordered manner. This morphology is characteristic of tobermorite,

and the XRD analysis (Fig. 8a) confirmed the precipitation of tobermorite on the GW surface.

Changes in the surface morphology of the GW for up to 7 days showed a similar trend to the precipitation layer formation reported in previous dissolution studies [9, 17]. According to Cagnon et al. [13], heterogeneous nucleation on the glass surface produces an amorphous spheroidal film, followed by the crystallization and growth of tobermorite-like aggregates. In the present study, the surface of the ${}^{80}_{14d}GW_{Na}$ sample and the globular-shaped precipitates exhibited EDS compositions summarized in Table 4, revealing that Ca/Si molar ratios significantly lower than the typical value of 0.8 for tobermorite. This suggests that, under NaOH solution conditions, the dissolved Ca from the glass surface served as the sole calcium ion source in the solution, resulting in incomplete crystallization and co-precipitation of substantial amounts of amorphous silica together with CSH during the early precipitation stage.

After 30 d, some ${}_{30d}{}^{80}GW_{Na}$ samples exhibited partial peeling of the platelet-structured layer, and renewed surface alteration was observed beneath the delaminated layer on the pristine glass surface. With increasing exposure time, the platelet-structured layer became progressively thicker, eventually peeling off from the surface as the interfacial bonding between the thickened porous layer and the GW surface gradually weakened. In addition, increasing mechanical stress acting on the layer may have contributed to the delamination behavior [4]. Similar delamination phenomena have been reported in previous studies on glass fiber degradation in alkaline NaOH environments, where such peeling behavior was shown to further promote continuous dissolution [3, 8].

Surface Alterations in CGW

No significant surface degradation of the GW was observed in the CGW solution until day 7. However, after seven days, a distinct change in surface morphology became evident in the SEM images. Figure 7 presents the evolution of the GW surface morphology after immersion in CGW for 7–30 days.

After seven days, the surface morphology began to change in a manner similar to that observed in the NaOH solution. The initially smooth surface transformed into a porous texture containing nanoscale pits at the glass-solution interface. In the ${}^{80}_{14d}GW_{CGW}$ sample, an additional precipitated layer was formed over the pre-existing porous layer (Fig. 7b). The onset of surface alteration after 7 days corresponds well with the dissolution behavior of Si ions.

Based on the EDS analysis of the surface and globular precipitates of the ${}^{80}_{14d}GW_{CGW}$ sample (Table 4), the surface composition did not differ significantly from that of the NaOH-immersed sample. However, the precipitates exhibited noticeably higher Ca content. The Ca/Si molar ratio of the precipitates was calculated to be 0.67, suggesting that they consisted of a Ca-Si amorphous aggregate containing tobermorite.

Precipitates and alteration layers forming on silicate glass surfaces are often reported to impart a protective effect [33, 34]. However, the deposits observed in this study exhibited a low Ca/Si ratio (~ 0.67), suggesting little to no passivation. Consistent with this observation, Marachechi et al. [17] reported that, in high-alkalinity solutions, soda-lime glass develops Ca–Si corrosion products with Ca/Si ratios of 0.54–0.78 on its surface; however, these phases do not provide protection against further glass dissolution.

Characterization of Precipitates (XRD)

The precipitates formed during GW dissolution vary depending on the composition of the glass and solution, pH, and the presence of carbon dioxide. Under accelerated degradation conditions, XRD analyses were conducted on samples retrieved at 7, 14, and 30 days from the three solutions. Except under the $Ca(OH)_2$ condition, in which no

Table 4 EDS results (wt%) of GW after 14 days—surface and precipitate compositions by solution, with corresponding Ca/Si ratios by weight and atomic percentage

	Original GW	$Ca(OH)_2$	CGW		NaOH	
	Surface	Surface	Surface	Precipitation	Surface	Precipitation
O	52.61	49.60	50.12	57.92	51.49	54.40
Si	29.28	33.54	32.84	19.49	32.33	29.92
Na	10.14	8.30	5.39	1.62	6.68	2.76
Ca	4.63	6.06	6.13	18.68	5.21	8.91
Mg	2.23	1.87	4.46	1.17	3.42	1.28
Al	1.10	N/D	1.06	1.12	0.86	1.28
Ca/Si (wt %)	0.158	0.181	0.187	0.958	0.161	0.298
Ca/Si (at %)	0.111	0.127	0.131	0.672	0.113	0.209

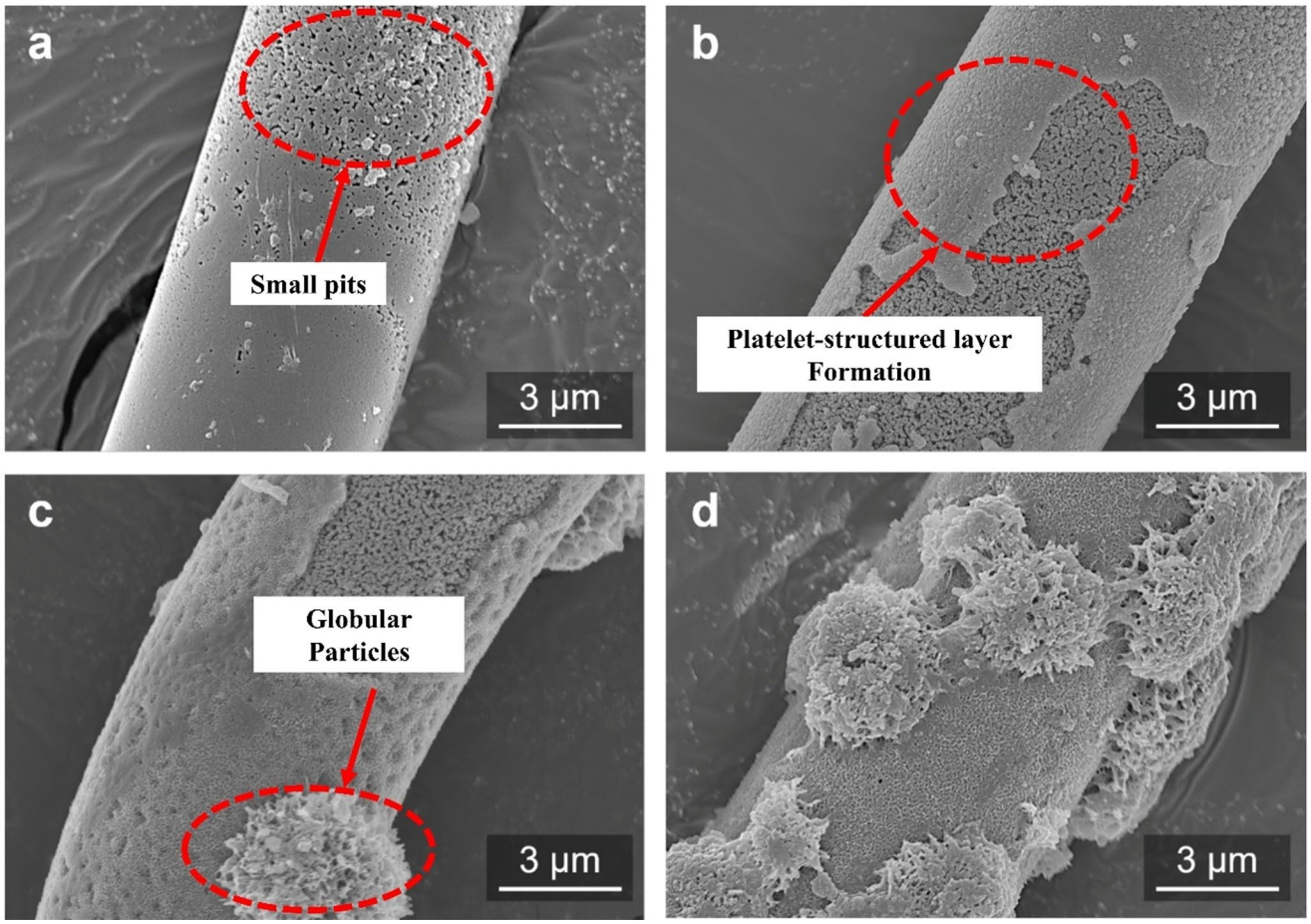

Fig. 7 SEM micrographs of glass wool fiber surfaces after accelerated degradation in CGW solution: (**a**) 7 d, (**b**) 14 d, (**c**) 20 d, and (**d**) 30 d

crystalline peaks were detected, the background-subtracted XRD patterns of GW for the NaOH and CGW solutions are presented in Fig. 8.

In the ${}^{80}_{7d}GW_{Na}$ specimen, diffraction peaks attributable to tobermorite ($Ca_5Si_6O_{16}{\cdot}4H_2O$, ICDD 00-019-1364)—the crystalline form of CSH—vaterite ($CaCO_3$, ICDD 00-024-0030), aragonite ($CaCO_3$, ICDD 00-005-0453), calcite ($CaCO_3$, ICDD 01-080-2793), and CSH ($Ca_{1.5}SiO_{3.5}{\cdot}$xH2O, ICDD 00-033-0306) were identified. Among these, vaterite, aragonite, and calcite are polymorphs of calcium carbonate known to form during the decalcification–polymerization of CSH. Generally, CSH is metastable under alkaline conditions; as decalcification proceeds, vaterite and aragonite first precipitate and subsequently transform into the thermodynamically more stable calcite. During this process, the initially formed CSH undergoes breakdown of Ca–O linkages and becomes Si-rich amorphous silica following the leaching of Ca^{2+}, which is consistent with our EDS results.

The XRD patterns of the ${}^{80}_{14d}GW_{Na}$ and ${}^{80}_{7d}GW_{Na}$ specimens exhibited no significant differences. However, in the ${}^{80}_{30d}GW_{Na}$ specimen, the vaterite and aragonite peaks were markedly reduced. Given that no additional CO_2 was supplied between 14 and 30 days, this suggests that the residual CO_2 was completely consumed, preventing further carbonation and resulting in transformation into stable calcite.

Consistent with the SEM observations, almost no crystalline peaks were detected in the ${}^{80}_{7d}GW_{CGW}$ specimen, whereas the ${}^{80}_{14d}GW_{CGW}$ specimen exhibited diffraction peaks corresponding to calcium carbonate polymorphs (vaterite, aragonite, and calcite) and tobermorite-type CSH phases, similar to those observed under NaOH conditions. After 30 days, a general decrease and broadening of diffraction peaks were observed for all precipitates, except calcite. This suggests that, under CGW solution conditions, the precipitation of CSH proceeded more slowly (after 7 days), whereas decalcification and carbonation reactions occurred more actively within a shorter time span. This mechanism can be attributed to the higher concentration of carbonate ions in the original CGW solution compared to NaOH. Although a complete theoretical consensus has not yet been reached, it is generally recognized that CSH with a lower Ca/Si ratio exhibits greater resistance to carbonation [35, 36]. In the NaOH solution, calcium ions were supplied

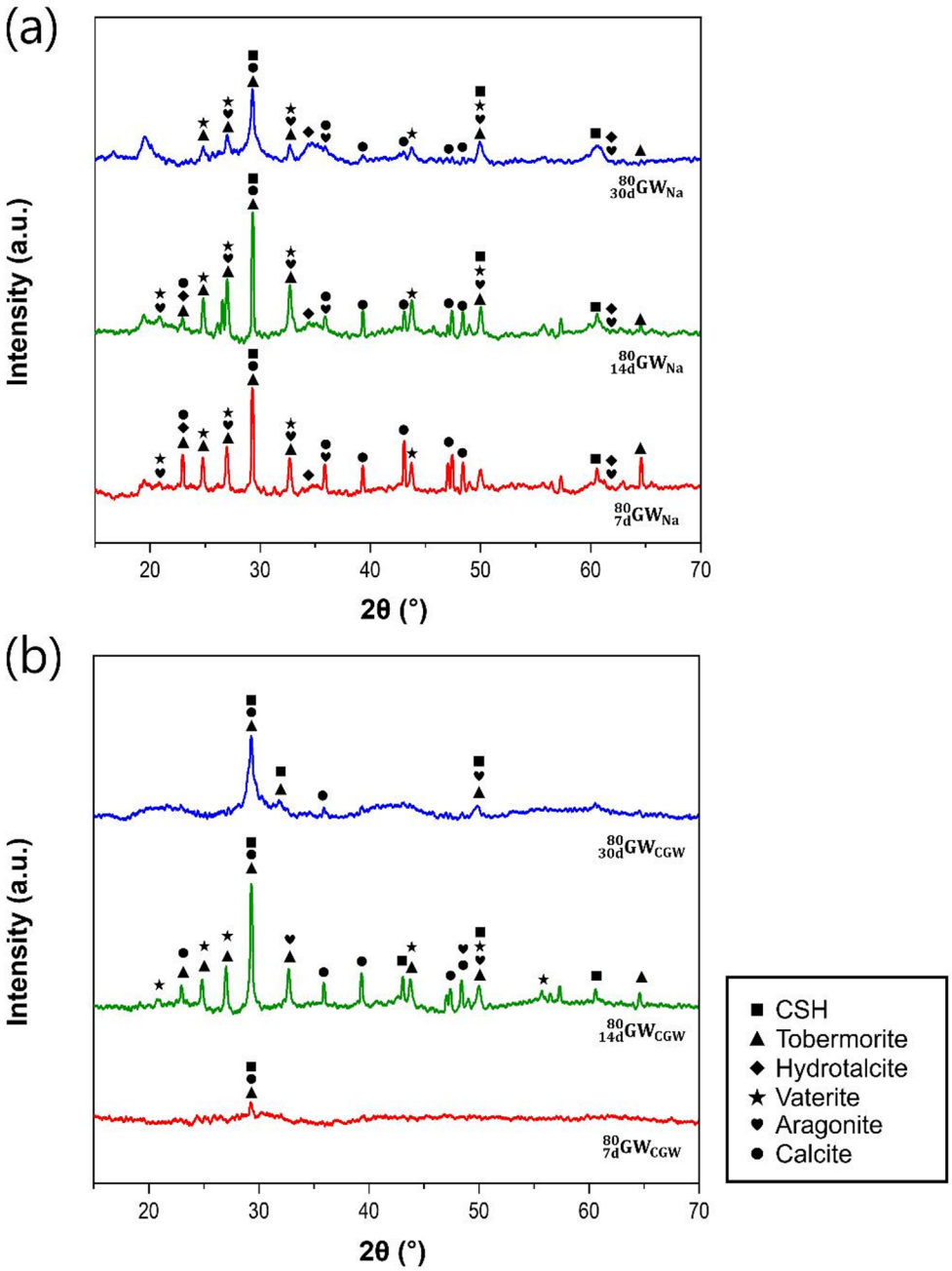

Fig. 8 XRD patterns of GW specimens obtained from the accelerated dissolution tests after 7, 14, and 30 days: (**a**) NaOH solution and (**b**) CGW solution

solely through the dissolution of glass wool; thus, the limited availability of Ca led to the formation of precipitates with low Ca/Si ratios.

The decalcification and carbonation of CSH identified from the XRD analysis indicated the possible transformation of CSH into a Ca–Si amorphous gel. Because silica gel is typically porous and loosely bound to the glass surface, it provides little passivation against glass degradation. In particular, under carbonate-rich CGW conditions, carbonate species promote interfacial instability through the decalcification and carbonation of CSH, thereby facilitating the progression of glass wool degradation.

Solution Chemistry and Dissolution Rate

Dissolution of Glass Wool in Various Alkaline Solutions

Figure 9 presents the ICP results for the concentrations of Si and Ca ions over 30 days in various alkaline solutions (NaOH, CGW, and $Ca(OH)_2$) under accelerated degradation conditions (80 °C).

Consistent with the SEM observations, Si rapidly leached from the GW surface in the NaOH solution from day 1, with a continuous increase in Si concentration up to day 30. During the initial stage (1–24 h), the slope of

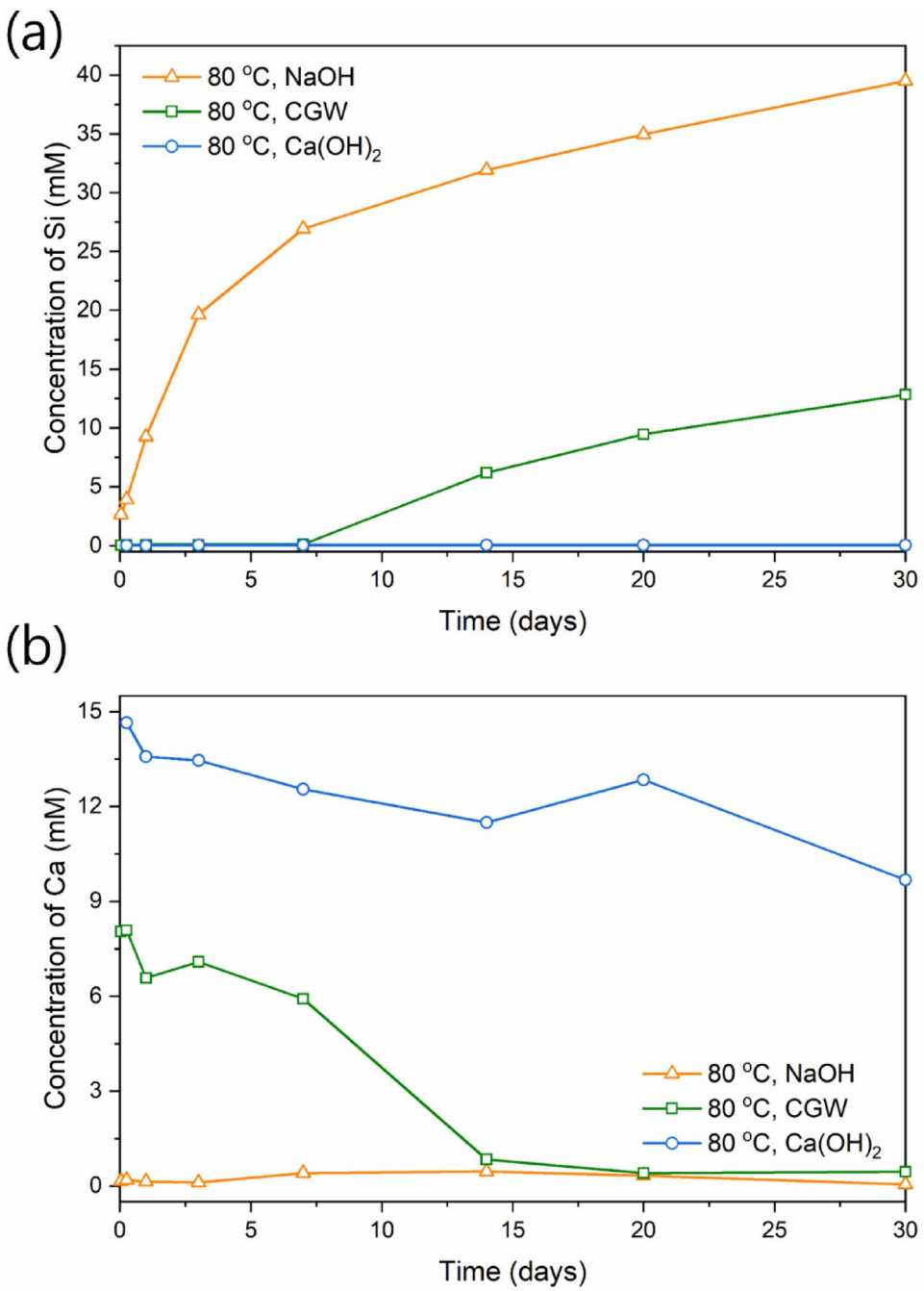

Fig. 9 Concentration variation of (**a**) Si and (**b**) Ca (mM) in various alkaline solution (pH 12.5) measured over 0–30 days

the Si concentration increase was steeper than in the later stage (7–30 d), which agrees with trends reported in previous glass dissolution studies [9]. In the early stage, glass dissolution proceeds at its maximum forward rate, resulting in a steep increase in Si concentration. As observed in the surface analyses, this rate gradually decreased as backward reactions—such as silica gel formation and secondary precipitation—began to occur. When a dense alteration layer forms on the glass surface or when Si ions in the solution approach saturation, thereby reducing the affinity for further dissolution, a rate drop occurs, and the dissolution rate eventually declines to a stage where additional dissolution becomes negligible. However, under the present experimental conditions of high pH, elevated temperature, and a large liquid-to-solid ratio, the high solubility of Si maintained a steady dissolution rate. Furthermore, although a precipitation layer was observed on the glass surface after seven days, the sustained linear increase in Si concentration indicated that this layer had little or no passivating effect on further dissolution.

In contrast, under identical conditions in the $Ca(OH)_2$ solution, no significant increase in Si concentration was

observed over 30 days. The Si concentration increased only slightly from 0.02 mM (0.576 ppm) at 12 h to 0.037 mM (1.03 ppm) at day 7, and remained nearly constant at 0.039 mM (1.08 ppm) at day 30, within the ICP measurement error range. This result indicates that hydroxide ion-driven network dissolution was largely suppressed in the $Ca(OH)_2$ solution, consistent with the surface morphology analysis results.

For the CGW solution, am intermediate behavior between NaOH and $Ca(OH)_2$ was observed. The Si concentration increased continuously but remained low (~0.1 mM) until day 7. However, after day 7, the Si concentration increased sharply, rising about 60-fold from 0.1 mM (2.62 ppm) at day 7 to 6.18 mM (173 ppm) at day 14. During the same period, the Ca concentration decreased markedly from 6 mM to 0.8 mM.

Combining these ICP results with the SEM observations and XRD patterns suggests that between days 7 and 14, extensive consumption of dissolved Ca ions occurred due to the continued precipitation of amorphous (or crystalline) CSH and concurrent carbonation (polymerization) reactions at the glass–solution interface.

Effect of Ca^{2+} Ion and Secondary Phase Evolution on Dissolution of Glass Wool

Under accelerated degradation conditions, a clear difference in the Si leaching rate was observed among the three solutions, despite having identical initial pH values. These results indicate that the concentration of dissolved Ca^{2+} exerts a strong inhibitory effect on the dissolution of glass wool. This inhibitory effect has been well documented in previous studies. In alkaline environments, glass dissolution is initiated by nucleophilic attack of OH^- ions on Si–O–Si bonds, resulting in bond cleavage and the formation of silanol groups (Reaction 6):

$$\equiv Si-OH + {}^{-}O-Si\equiv \rightarrow \equiv Si-O-Si\equiv +OH^- \quad (6)$$

As dissolution proceeds, the concentration of dissolved Si increases, and the consumption of OH^- causes a slight decrease in pH. This change in solution chemistry promotes partial re-polymerization of the silicate network through condensation reactions, leading to reformation of Si–O–Si bonds (Reaction 7):

$$\equiv Si-OH + {}^{-}O-Si\equiv \rightarrow \equiv Si-O-Si\equiv +OH^- \quad (7)$$

At pH > 10, Ca^{2+} ions promote additional recondensation of siloxane bonds by bridging adjacent silanol groups, forming Ca–Si linkages that eventually restore siloxane connectivity (Reactions 8–9):

$$2\equiv Si-OH + Ca(OH)_2 \rightarrow \equiv Si-O-Ca-O-Si\equiv +2H_2O \quad (8)$$

$$\equiv Si-O-Ca-O-Si\equiv +2H_2O \rightarrow \equiv Si-O-Si\equiv +Ca^{2+}+2OH^- \quad (9)$$

Through these reactions, Ca^{2+} penetrates the surface layer, densifies the silicate network, and forms a diffusion barrier that retards further dissolution. In addition, when the concentration of dissolved silicate becomes sufficiently high, it reacts with Ca^{2+} to form calcium silicate hydrate (CSH), further reducing the available Ca^{2+} and altering surface reactivity. In the $Ca(OH)_2$ solution, CSH formation was not detected in the XRD analysis; however, the initially high Ca^{2+} concentration appears to have promoted the rapid densification of the glass network at the GW–solution interface, resulting in the very low dissolved-Si concentrations observed during the early stage of the experiment.

Similarly, the CGW solution contained a high Ca concentration (348 ppm), which likely delayed glass dissolution through a comparable surface-densification process. However, the subsequent renewed dissolution observed in CGW reflects a coupled sequence of geochemical processes associated with Ca consumption and secondary phase evolution. After 7 days, the concentration of dissolved Ca^{2+} decreased rapidly, most likely due to its consumption in the formation of amorphous CSH and carbonate phases. As Ca became depleted, the barrier effect on the glass wool surface was progressively diminished, leading to a rapid acceleration of degradation.

In the CGW solution, the presence of CO_2 in the container and the higher carbonate (CO_3^{2-}) concentration compared with the $Ca(OH)_2$ solution further favored calcium carbonate precipitation, leading to faster depletion of dissolved Ca^{2+} in bulk solution. Carbonate precipitation not only reduced the aqueous Ca concentration but may also have contributed to partial decalcification of interfacial CSH. As the Ca concentration decreased, the extent of siloxane re-condensation diminished, accelerating hydroxyl-ion-driven dissolution of the glass network. During this dissolution process, the dissolved silicate reacted with Ca^{2+}, forming additional CSH and consuming more Ca^{2+}. The newly formed CSH layer and associated precipitates likely served as heterogeneous nucleation sites for calcite, thereby contributing to the observed decrease in dissolved Ca^{2+} concentration.

This sequence of reactions likely occurred between 7 and 14 days, and the sharp drop in Ca^{2+} concentration— from 6 mM (at 7 days) to 0.8 mM (at 14 days)—is interpreted as a self-accelerating process. A similar trend was reported by H. Maraghechi et al., who investigated the corrosion of soda–lime glass plates in three solutions: (1) 1 M NaOH without Ca^{2+}, (2) 1 M NaOH saturated with $Ca(OH)_2$, and (3)

1 M NaOH containing excess solid $Ca(OH)_2$. Their results showed negligible Si leaching under Condition (3), delayed corrosion under Condition (2), and renewed dissolution as the concentration of dissolved Ca^{2+} decreased—findings consistent with those of this study [17].

Figure 10 presents the concentration profiles of Ca and Na ions in the CGW solution at 80 °C. Because Na^+ is highly soluble and only minimally incorporated into secondary phases, its concentration serves as a reliable indicator of ion exchange and silicate network dissolution at the glass surface. The Na concentration remained approximately constant at 2 mM (≈60 ppm) during the first 7 days, suggesting that surface densification suppressed ion diffusion and dissolution. After 7 days, the observed decline in Ca concentration corresponded to the onset of significant ion diffusion, further supporting this interpretation.

Dissolution Rate of Glass Wool in Various Alkaline Conditions

Because Si (or SiO_2) is the primary network-forming element in silicate glass, the overall dissolution rate of the glass network can be determined from the Si leaching rate (Eq. 3). The concentration of dissolved Si in the solution was first used to calculate the normalized mass loss (NL, $\mu\, g/cm^2$) according to Eq. 1. Considering the general corrosion behavior of glass, the dissolution process was divided into two stages: the initial stage (1–12 h) and the later stage (7–30 d). In the case of the $Ca(OH)_2$ solution, no measurable change in Si concentration was observed; therefore, it was excluded from further analysis. Under accelerated dissolution experiments, the stage-dependent normalized mass loss of Si ions in the NaOH and CGW solutions are presented in Fig. 11.

Under accelerated degradation conditions, the NL_{Si} exhibited a linear trend over time in both the initial and later stages for the NaOH and CGW solutions. To compare

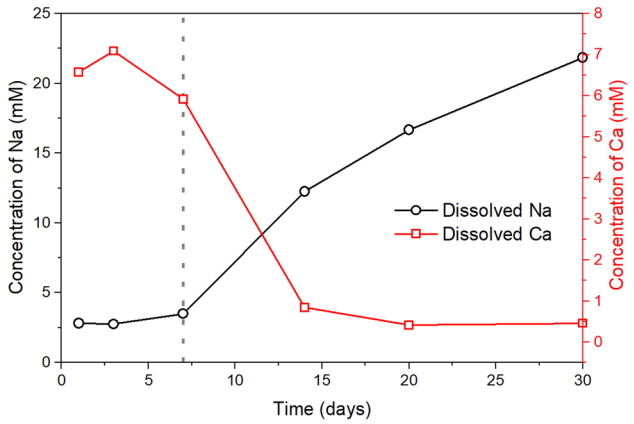

Fig. 10 Changes in Ca and Na concentrations in CGW solution over time during the accelerated degradation experiment

the normalized dissolution rates (μg/cm²/h) under different experimental conditions, linear regression was applied to determine the slopes for both stages (Table 5). In the accelerated degradation experiment with the NaOH solution, the normalized dissolution rate was calculated as 0.254 μg/cm²/h (R^2 = 0.937) during the initial stage and 0.0331 μg/cm²/h (R^2 = 0.993) during the later stage. In the CGW solution, the initial dissolution rate was significantly lower—0.00174 μg/cm²/h (R^2 = 0.971)—more than two orders of magnitude lower than that in the NaOH solution. However, in the later stage (after 7 days), a similar rate of 0.0330 μg/cm²/h (R^2 = 0.965) was obtained.

In general, the dissolution rate of glass exhibited an initial rapid increase, reaching a maximum forward dissolution rate during the early stage. Subsequently, a rate drop occurred as backward reactions such as silica gel recondensation and secondary precipitation progressed, depending on the surrounding environment. This drop typically represents a transition from an initially elevated rate to a residual regime with a low but finite rate [37].

In this study, a reduction of approximately two orders of magnitude in the normalized dissolution rate was observed during the transition from the initial stage (1–10 h) to the later stage (7–30 days). However, in the later stage, no additional rate drop occurred, and linear dissolution behavior was maintained. This trend has also been widely reported in other studies investigating glass dissolution under high-alkalinity conditions, where linearity was preserved regardless of variations in solution composition (except for high Ca concentration), glass type, or temperature [6, 11, 17]. This behavior provides strong evidence that the dominant driving force of dissolution is the hydrolysis reaction between hydroxyl ions and the glass network. Furthermore, under these conditions, the elevated solubility of Si species prevents the solution from reaching Si saturation, maintaining a high-affinity state and thereby enabling long-term linear dissolution.

In contrast, in the CGW solution, the dissolution rate in the later stage was higher than that in the initial stage. As mentioned above, the initially high Ca concentration in the CGW solution promoted densification of the altered layer, suppressing glass network dissolution and making interdiffusion the rate-determining process. Therefore, the increase in dissolution rate observed in the later stage indicates that after approximately seven days, the rapid decrease in Ca concentration due to CSH formation and carbonation caused the Ca–Si passivation layer to lose its protective function, allowing hydrolysis to again become the dominant dissolution mechanism.

The similar dissolution rates observed in both solutions suggest that the precipitation layer identified by SEM analysis did not significantly hinder contact between the solution

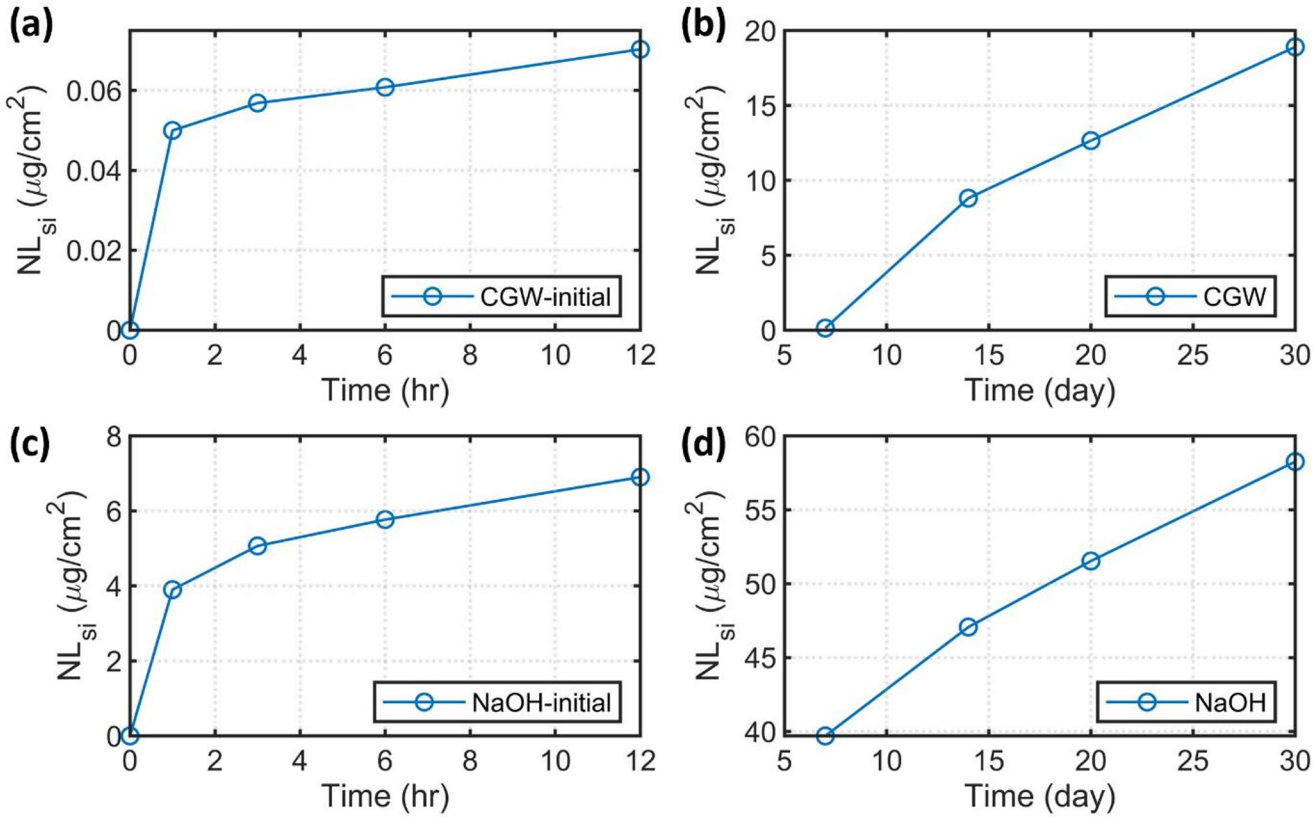

Fig. 11 Normalized mass loss of Si under accelerated degradation conditions: initial stage (1–12 h) in (**a**) CGW and (**c**) NaOH solutions; later stage (7–30 days) in (**b**) CGW and (**d**) NaOH solutions

Table 5 Normalized dissolution rates of GW in accelerated degradation conditions

Experimental condition	Normalized dissolution rate ($\mu g/cm^2/h$)	
	Initial stage	later stage
NaOH, 80 °C	0.254	0.0331
CGW, 80 °C	0.00174	0.0330

and the glass surface, and that both systems exhibited comparable dissolution kinetics. Bashir et al. [6] evaluated the kinetics of glass dissolution in different high-alkalinity solutions (NaOH and KOH) using zero-order and shrinking-cylinder models. Under identical concentration and temperature conditions, the activation energy (E_a) derived from the zero-order model was lower for NaOH than for KOH, indicating that more energy is required for hydroxyl ions to be transported to the reaction interface in NaOH. However, similar activation energies were obtained from the shrinking-cylinder model for both alkaline solutions, implying that the energy required for surface hydrolysis was largely independent of the alkaline medium.

As shown in Fig. 10, the concentration of Na^+ increased markedly as Ca^{2+} ions in the solution were depleted. Considering the high Na content and solubility of soda–lime glass, the Na concentration near the surface was expected to be greater than that in the bulk solution. Accordingly, when Ca is depleted from the solution and Na becomes highly enriched during soda–lime glass dissolution, alteration resumption may occur, reactivating dissolution rates comparable to those observed in NaOH solutions.

Estimated Degradation in Repository Conditions

The accelerated dissolution experiments described above confirmed that sustained dissolution can occur in highly alkaline solutions. Accordingly, from a conservative standpoint, glass wool disposed of in domestic repositories is assumed to undergo continuous dissolution. The dissolution rate and time to complete dissolution were calculated under NaOH and CGW conditions using Eqs. (4) and (5), respectively. To estimate repository-relevant parameters (e.g., ν and $k_{dissolution}$), an additional 30-day test was conducted at 20 °C under the same solution chemistry as the accelerated degradation experiments, representing the temperature conditions expected in domestic repositories. The accelerated tests were therefore used to confirm the persistence of dissolution behavior, while quantitative lifetime estimates were obtained from the 20 °C data. Since the calculation is based on the 20 °C dataset, no temperature dependent

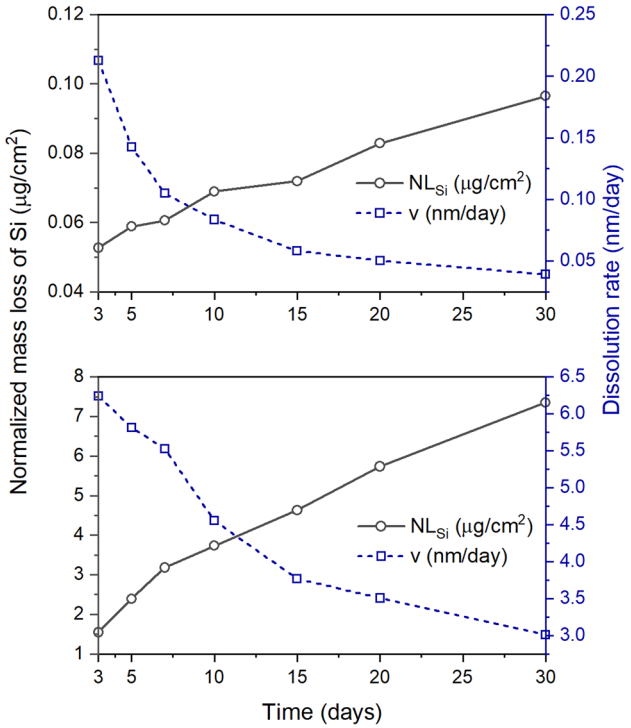

Fig. 12 Normalized mass loss of Si ($\mu\, g/cm^2$) and global dissolution rate (v, nm/day) at 20 °C: (**a**) CGW solution, (**b**) NaOH solution

Table 6 Estimated complete dissolution time of GW under repository-simulated conditions (days)

Experiment condition	$t_{dissolution}$
NaOH (pH 12.5), 20 °C	1,117 (about 3.06 year)
CGW (pH 12.5), 20 °C	78,008 (about 213 year)

extrapolation was applied. Only the NaOH and CGW solution conditions are reported because the $Ca(OH)_2$ condition was excluded; the cumulative dissolved Si did not exhibit a consistent increase either in the accelerated degradation tests or at 20 °C (Fig. 12).

At 20 °C, consistent with the accelerated degradation experiments, the normalized Si mass loss increased approximately linearly with time, with no apparent rate drop. The global dissolution rate, ν, decreased progressively with time over the observation period. Because different values of the dissolution rate constant ($k_{dissolution}$) can arise depending on glass composition and early-stage dissolution behavior, the present work follows the methodology proposed by Campopiano et al. [26]: after day 14, $k_{dissolution}$ was evaluated from the three-point mean of the dissolution rate (ν) measured at 15, 20, and 30 days.

Using the average dissolution rates derived above, the dissolution rate constant $k_{dissolution}$ of GW at 20 °C in pH 12.5 NaOH was calculated by Eq. (4) as 33.989 ng cm^{-2} h^{-1}. Under the CGW solution conditions, a dissolution rate of 0.049 ng cm^{-2} h^{-1} was obtained, which was approximately 70 times lower than that measured under NaOH conditions at the same pH. Applying Eq. (5) with a mean fiber diameter of d = 7.66 μm and density ρ = 2.38 g/cm^3, the corresponding times to complete dissolution were obtained. The results are summarized in Table 6.

Under repository-simulated conditions, the complete dissolution time of glass wool was estimated to be approximately 3.06 years in NaOH solution and 213 years in CGW solution. Similar to the accelerated dissolution experiments, the much lower dissolution rate in the CGW condition—representing the composition of groundwater expected in a repository environment—resulted in a substantially longer dissolution time. Because the reaction proceeds very slowly at low temperatures, no resumption of alteration was observed. Furthermore, in domestic repository environments, alkaline groundwater is expected to exist in a flow-through state rather than under static conditions. Under such conditions, the Ca concentration in the solution would likely remain high, thereby maintaining the passivated Ca–Si layer formed on the glass surface. Nevertheless, if contact between the glass wool and the solution persists within confined spaces or under limited flow conditions, accelerated dissolution could occur. Therefore, this potential scenario should be carefully considered in long-term safety assessments of disposal systems.

Summary and Conclusion

This study investigated the degradation behavior of insulation-grade glass wool—used for thermal insulation in nuclear power plants—under strongly alkaline conditions through two complementary experiments: (i) accelerated dissolution tests to evaluate the evolution of dissolution behavior under high pH and temperature, and (ii) repository-simulated tests to quantify the dissolution rate under vault-type repository chemistries. Three solutions with identical pH values were employed to assess the effect of solution chemistry on glass wool dissolution. SEM, XRD, and ICP-OES analyses were performed on both the specimens and the solutions to characterize dissolution behavior and precipitation products. The key conclusions are summarized as follows:

- The concentration of Ca in alkaline solutions, and its interaction with dissolved silica, strongly influenced glass dissolution behavior.
- In Ca-enriched solutions, gel densification at the glass surface formed a passivating layer that suppressed further dissolution.
- In accelerated CGW conditions, where Ca is consumed through carbonate reactions and secondary precipitation,

dissolution becomes hydrolysis-controlled, resulting in dissolution rates comparable to NaOH at the same pH.

- Under strongly alkaline conditions, precipitates formed a continuous, percolated nanoparticulate layer mainly composed of amorphous CSH and silica. Due to its high porosity and low Ca content, this layer does not effectively hinder ion transport, and no reduction in dissolution rate was observed.
- In carbonate-containing systems (e.g., vault-type repositories), persistent decalcification of CSH prevents the formation of a dense, passivating layer.
- Under conservatively simulated disposal conditions (CGW solution, 20 °C), the dissolution rate constant was 0.049 ng cm^{-2} h^{-1}, corresponding to an estimated complete-dissolution time of about 213 years for the tested fiber geometry.
- If highly alkaline solution remains near-stagnant or confined, progressive Ca depletion may trigger resumption of glass alteration, potentially increasing the dissolution rate by ~ 70 times.

Acknowledgements This work was supported by the Korea Institute of Energy Technology Evaluation and Planning(KETEP) and the Ministry of Trade, Industry & Energy(MOTIE) of the Republic of Korea (RS-2023-00235182).

Funding Open Access funding enabled and organized by Ulsan National Institute of Science and Technology (UNIST)

Declarations

Conflict of interest The authors declare that they have no known competing financial interests or personal relationships that could have appeared to influence the work reported in this paper.

References

1. J. Kośny, D.W. Yarbrough (eds.), *Thermal Insulation and Radiation Control Technologies for Buildings*, Green Energy Technol. (Springer, Cham, 2022). https://doi.org/10.1007/978-3-030-98693-3
2. R. Kolbe, E. Gahan, *Survey of Insulation Used in Nuclear Power Plants and the Potential for Debris Generation, NUREG/CR-2403, Suppl* Sandia Natl. Lab. (NM, and Burns & Roe, Inc., Oradell, NJ, 1982), pp. SAND82–0927. 1Albuquerque
3. C. Scheffler, T. Förster, E. Mäder, G. Heinrich, S. Hempel, V. Mechtcherine, J. Non-Cryst Solids. **355**(52–54), 2588–2595 (2009). https://doi.org/10.1016/j.jnoncrysol.2009.09.018
4. Q. Wang, Y. Ding, N. Randl, Constr. Build. Mater. **272**, 121670 (2021). https://doi.org/10.1016/j.conbuildmat.2020.121670
5. S. Rossignol, S.S. Kouassi, J. Andji, J.-P. Bonnet, Ceramics-Silikáty. **54**(1), 1–6 (2010). https://www.researchgate.net/publication/268400656
6. S.T. Bashir, L. Yang, J.J. Liggat, J.L. Thomason, J. Mater. Sci. **53**, 1710–1722 (2018). https://doi.org/10.1007/s10853-017-1627-z
7. M.S. Kim, S.C. Han, J.I. Yun, Nucl. Eng. Technol. **56**(9), 3942–3949 (2024). https://doi.org/10.1016/j.net.2024.04.041
8. C. Tang, H. Jiang, X. Zhang, G. Li, J. Cui, *Materials* 11(8), 1381 (2018). https://doi.org/10.3390/ma11081381
9. R. Ramaswamy, J. Yliniemi, M. Illikainen, Cem. Concr Res. **160**, 106922 (2022). https://doi.org/10.1016/j.cemconres.2022.106922
10. S. Mercado-Depierre, F. Angeli, F. Frizon, S. Gin, J. Nucl. Mater. **441**(1–3), 402–410 (2013). https://doi.org/10.1016/j.jnucmat.2013.06.023
11. E.C. La Plante, T. Oey, Y.H. Hsiao, L. Perry, J.W. Bullard, G. Sant, J. Phys. Chem. C **123**(6), 3687–3695 (2019). https://doi.org/10.1021/acs.jpcc.8b12076
12. T. Förster, C. Scheffler, E. Mäder, G. Heinrich, D.A. Jesson, J.F. Watts, Appl. Surf. Sci. **322**, 78–84 (2014). https://doi.org/10.1016/j.apsusc.2014.10.058
13. B. Cagnon, S. Gin, M. Cabié, D. Daval, J. Nucl. Mater. **603**, 155426 (2025). https://doi.org/10.1016/j.jnucmat.2024.155426
14. L. Peng et al., Cem. Concr Compos. **137**, 104909 (2023). https://doi.org/10.1016/j.cemconcomp.2022.104909
15. M. Mejdi, W. Wilson, M. Saillio, T. Chaussadent, L. Divet, A. Tagnit-Hamou, Cem. Concr Res. **123**, 105790 (2019). https://doi.org/10.1016/j.cemconres.2019.105790
16. S. Mercado-Depierre, M. Fournier, S. Gin, F. Angeli, J. Nucl. Mater. **491**, 67–82 (2017). https://doi.org/10.1016/j.jnucmat.2017.04.043
17. H. Maraghechi, F. Rajabipour, C.G. Pantano, W.D. Burgos, Cem. Concr Res. **87**, 1–13 (2016). https://doi.org/10.1016/j.cemconres.2016.05.004
18. P. Frugier et al., J. Nucl. Mater. **380**(1–3), 8–21 (2008). https://doi.org/10.1016/j.jnucmat.2008.06.044
19. M. Fournier, T. Ducasse, A. Pérez, A. Barchouchi, D. Daval, S. Gin, J. Nucl. Mater. **524**, 21–38 (2019). https://doi.org/10.1016/j.jnucmat.2019.06.029
20. W. Kurdowski, Cem. Concr Res. **34**(9), 1555–1559 (2004). https://doi.org/10.1016/j.cemconres.2004.03.023
21. N. Krautwurst et al., Chem. Mater. **30**(9), 2895–2904 (2018). https://doi.org/10.1021/acs.chemmater.7b04245
22. Z. Zhao et al., Materials. **10**(6), 597 (2017). https://doi.org/10.3390/ma10060597
23. M. Jin et al., J. Mater. Sci. **57**, 19260–19279 (2022). https://doi.org/10.1007/s10853-022-07857-7
24. Y. Li et al., J. CO2 Util. **35**, 303–313 (2020). https://doi.org/10.1016/j.jcou.2019.10.001
25. A.S.T.M. International, *Test Methods for Determining Chemical Durability of Nuclear, Hazardous, and Mixed Waste Glasses and Multiphase Glass Ceramics: The Product Consistency Test (PCT)*, ASTM C1285-21ASTM International, West Conshohocken, PA, (2021). https://doi.org/10.1520/C1285-21
26. A. Campopiano et al., Regul. Toxicol. Pharmacol. **70**(1), 393–406 (2014). https://doi.org/10.1016/j.yrtph.2014.05.023

27. S. Thélohan, A. de Meringo, *Environ. Health Perspect.* 102, Suppl. 5, 91–96 (1994). https://doi.org/10.2307/3432066
28. C.A. Utton, R.J. Hand, P.A. Bingham, N.C. Hyatt, S.W. Swanton, S.J. Williams, J. Nucl. Mater. **435**(1–3), 112–122 (2013). https://doi.org/10.1016/j.jnucmat.2012.12.032
29. S. Gin et al., Geochim. Cosmochim. Acta. **151**, 68–85 (2015). https://doi.org/10.1016/j.gca.2014.12.009
30. S. Zhang, Y. Liu, Geochem. J. **48**(2), 189–205 (2014). https://doi.org/10.2343/geochemj.2.0298
31. A. Helebrant, H. Hradecká, B. Holubová, L. Brázda, M. Netušilová, Z. Zlámalová-Cílová, Ceramics-Silikáty. **61**(2), 163–171 (2017). https://doi.org/10.13168/cs.2017.0012
32. P. Wang et al., Constr. Build. Mater. **391**, 131757 (2023). https://doi.org/10.1016/j.conbuildmat.2023.131757
33. P. Frugier, T. Chave, S. Gin, J.E. Lartigue, J. Nucl. Mater. **392**(3), 552–567 (2009). https://doi.org/10.1016/j.jnucmat.2009.04.024
34. Y. Minet, B. Bonin, S. Gin, P. Frugier, J. Nucl. Mater. **404**(3), 178–202 (2010). https://doi.org/10.1016/j.jnucmat.2010.07.015
35. T. Ishida, Y. Ito, K. Kawai, *Cement science and concrete technology.* 67(1), 487–494 (2013). https://doi.org/10.14250/cement.67.487
36. J. Li, Q. Yu, H. Huang, S. Yin, Materials. **12**(8), 1268 (2019). https://doi.org/10.3390/ma12081268
37. C.L. Corkhill, N.J. Cassingham, P.G. Heath, N.C. Hyatt, Int. J. Appl. Glass Sci. **4**(4), 341–356 (2013). https://doi.org/10.1111/ijag.12042